Power Swing-Induced Maloperation in Distance Protection with Large Data Center Load

Saeed Sanati
Grid Automation, GE Vernova
Markham, ON, Canada
Laval University
Quebec City, QC, Canada
saeed.sanati@gevernova.com

Arash Mahari
Grid Automation
GE Vernova
Markham, ON, Canada
arash.mahari@gevernova.com

Mikhail Martynov
Grid Automation
GE Vernova
Markham, ON, Canada
Mikhail.Martynov@gevernova.com

Palak Parikh
Grid Automation
GE Vernova
Markham, ON, Canada
Palak.Parikh@gevernova.com

***Abstract*—The rapid growth of large-scale data centers introduces new challenges for conventional impedance-based distance protection. Their highly dynamic and computation-driven load behavior can mimic short-circuit conditions, causing the apparent impedance to encroach on relay trip characteristics. In this work, detailed data center load models—representing large training, small training, and fine-tuning AI workloads—are developed to reproduce realistic power variability. A simulation framework is established to track both the apparent impedance and its instantaneous rate of change, enabling analysis of impedance trajectories and movement speed in the R–X plane. The study utilizes a realistic test system to demonstrate that data center load surges can drive the impedance rapidly into the mho zone (evading power swing blocking), after which its movement slows dramatically, creating conditions indistinguishable from a short circuit and leading to maloperation. The analysis specifically incorporates inner and outer blinders to evaluate the time-based crossing logic. These findings highlight the need for enhanced and adaptive protection schemes tailored to emerging large-load environments.**

***Index Terms*—Data Centers, distance protection, power swing, impedance tracking, load encroachment, adaptive protection, high-speed loads, AI workloads, relay maloperation, dynamic load modeling.**

I. Introduction

The integration of data centers into the power grid introduces unique challenges to power system protection. Understanding their dynamic behaviors, improving load modeling, and optimizing protection schemes are crucial steps in ensuring grid reliability. As the demand for data processing continues to grow, addressing these challenges will be essential for maintaining the stability and resilience of the power system [1].

Data centers differ fundamentally from traditional industrial or commercial loads. Their use of switch-mode power supplies (SMPS), uninterruptible power supplies (UPS), and variable frequency drives (VFDs) introduces fast transients, broad harmonic spectra, and stochastic loading patterns [2]–[4]. Table I compares data centers with other typical fast-changing loads found in industrial and utility systems. Each of these load types introduces transient current and voltage distortions, but the mechanisms and their protection implications vary significantly [2]–[5].

Unlike traction systems or HVDC loads, data centers operate with thousands of parallel SMPS and UPS modules, creating simultaneous high-frequency switching events [2], [3].

TABLE I
COMPARISON OF DATA CENTERS WITH OTHER FAST-CHANGING LOADS

Load Type	Transient Source	Predictability	Protection Impact
Motor starting	Magnetic inrush	Predictable	Inrush currents handled via delay or restraint
Arc furnace	Arc re-ignition	Quasi-random	Impedance fluctuation handled via filters
HVDC/VFD	Converter control	Deterministic	Directional and harmonic blocking used
Traction systems	Regeneration	Periodic	Reverse-power logic
Data centers	Aggregated SMPS + UPS	Stochastic, synchronized bursts	Causes simultaneous di/dt, dv/dt, PF swings, harmonic distortion

Fast-switching data center loads introduce steep di/dt, rapid P–Q steps, and elevated wideband harmonic content that stress both the measurement chain and protective algorithms [2], [3], [6]. Instantaneous and time-overcurrent elements can misoperate when short-duration current spikes exceed pickup before conventional filtering or intentional delays respond [5]. Directional and distance elements are vulnerable to rapid power-factor swings and waveform distortion that perturb phasor estimation and polarizing signals, leading to direction misclassification and distance overreach/underreach [7], [8]. Differential protections can see transient operate currents from CT saturation and localized high-frequency pulses that outpace restraint logic. Frequency-based elements (e.g., ROCOF) can falsely indicate islanding or generation loss when large, rapid load steps induce localized df/dt in weak grids. Power-quality protections may also alarm or trip on transient harmonic bursts. Underlying many of these mechanisms are instrumentation limits: CT/PT bandwidth and saturation behavior govern the fidelity of the relay inputs during wideband, nonstationary transients [9].

This paper focuses on characterizing power swing–induced maloperation of impedance-based distance protection in power systems supplying large data center loads. Using data center load models parameterized by realistic AI workload profiles

979-8-3315-8138-1

TABLE II
TYPICAL RANGES OF LOAD CHANGES IN DATA CENTERS

Parameter	Typical Range	Extreme Case	Time Window
Load step (ΔP)	10–500 kW	5–10 MW	1–100 ms
di/dt	50–600 A/ms	more than 1000 A/ms (UPS bypass)	less than 20 ms
dv/dt	1–10 V/μs	up to 20 V/μs	less than 5 ms
THD	5–15% (normal)	20–30% (transient)	less than 1 s

(large training, small training, and fine-tuning), the study simulates apparent impedance trajectories and their instantaneous rate of change to quantify the propensity for load encroachment and incorrect tripping during power swings. The analysis incorporates inner and outer blinders to evaluate the time-based crossing logic. The analysis is intended to provide practical insight and setting guidance for protection engineers planning or operating lines with high data center penetration.

II. Data Centers and Impedance-Based Protection

The integration of large data centers into modern power grids presents evolving challenges for protection engineers, particularly for single-node-measurement-based functions such as distance protection and its related functions. For example, integrating large data centers affects Power Swing Blocking (PSB). PSB is intended to block distance elements during slow, oscillatory impedance movement that follows major system disturbances [8]. These can excite oscillations in weak or lightly damped networks, but they are not themselves power swings and would only threaten synchronism when the load step is large relative to the local short circuit strength and inertia [1], [10].

Moreover on PSB, the key point is that existing schemes are designed to block on slow impedance trajectories and to avoid blocking on fast movements typical of faults. Because PSB intentionally ignores fast impedance changes, a sudden data center load change will not be blocked as a swing. If the steps are large enough, the apparent impedance can move toward the origin and into a distance zone, most commonly a long reach Zone 3. This risk is amplified when voltage sags during the step, which further shrinks the apparent impedance, and when zone characteristics are mho circles that extend into the high-power-factor load region.

Given these, achieving a robust performance requires studies with realistic models and test validation. Although most protection functions are phasor based, studies should be performed in both domains: phasor domain, including transient stability, and EMT simulations.

Table II summarizes the typical magnitudes of voltage, current, and harmonic variations observed in data center operations. These ranges help define the envelope within which protection schemes must remain secure and stable.

While the previous Table II provides magnitude estimates, Table III decomposes the load changes by type and operational origin, giving a detailed picture of multi-scale events relevant to protection studies.

The protection implication is that relays must maintain coordination over events ranging from microsecond-level device switching to multi-second facility-level ramps. Relay filtering and coordination settings should account for the inertia-free nature of these electronic loads, which can transition between states much faster than traditional rotating machinery [11], [12].

III. Stochastic Data Center Load Modeling for Protection Studies

Modern data centers, particularly those hosting large-scale artificial intelligence (AI) workloads, exhibit rapidly varying and non-stationary power demand. The stochastic and intermittent characteristics of AI training and fine-tuning cycles lead to fast variations in current magnitude and phase, causing the apparent impedance seen by protective relays to drift dynamically within and across protection zones. To capture these dynamics, a time-domain stochastic load model was developed based on workload-level power demand profiles.

A. Load Model Principles

The total AI computing load is represented as the sum of several concurrent workloads: one large-scale training process, multiple smaller training processes, and several fine-tuning tasks. Each workload alternates between high-power (*up-phase*) and low-power (*down-phase*) operation. The transition times and magnitudes follow Gaussian and uniform distributions to emulate the variability of processor utilization and cooling system response. For the i^{th} training workload, the total cycle duration is modeled as

$$T_{\mathrm{tr},i} = \frac{1}{f_0(1+\xi_i)}, \tag{1}$$

where f_0 is the nominal workload frequency and $\xi_i \sim \mathcal{N}(0, \sigma_\xi^2)$ introduces stochastic frequency variation. The ratio of the active (up-phase) to total cycle time is sampled from a uniform distribution,

$$r_{\mathrm{tr},i} \sim \mathcal{U}(r_{\min}, r_{\max}), \tag{2}$$

yielding

$$T_{\mathrm{up},i} = r_{\mathrm{tr},i} T_{\mathrm{tr},i}, \qquad T_{\mathrm{down},i} = (1 - r_{\mathrm{tr},i}) T_{\mathrm{tr},i}. \tag{3}$$

During each phase, the instantaneous power demand is modeled as

$$P_{\mathrm{up},i}(t) = P_{\mathrm{tr}}\big(1 + \delta_{\mathrm{up},i} + \eta_{\mathrm{up}}(t)\big), \tag{4}$$

$$P_{\mathrm{down},i}(t) = P_{\mathrm{tr}}\big(1 - \delta_{\mathrm{down},i} + \eta_{\mathrm{down}}(t)\big), \tag{5}$$

where $\delta_{\mathrm{up},i}$ and $\delta_{\mathrm{down},i}$ represent inter-cycle deviations in up- and down-phase power levels, modeled as Gaussian random variables:

$$\delta_{\mathrm{up},i} \sim \mathcal{N}(0, \sigma_\delta^2), \tag{6}$$

$$\delta_{\mathrm{down},i} \sim \mathcal{N}(\mu_\delta, \sigma_\delta^2), \tag{7}$$

and $\eta_{\mathrm{up}}(t)$, $\eta_{\mathrm{down}}(t)$ denote intra-phase fluctuations caused by micro-scale computational dynamics and cooling load interactions.

979-8-3315-8138-1

TABLE III
LOAD CHANGE TIME SCALES IN DATA CENTERS

Type of Event	Typical Magnitude	Time Scale	Cause / Description
Individual Server Power Step	100–500 W	<1 ms – 10 ms	CPU/GPU switching, core activation, or load spike
Rack or Cluster Load Step	10–50 kW	10–100 ms	Many servers ramp up simultaneously (e.g., AI inference job)
UPS DC Bus Response	Smooths within 5–20 ms	5–20 ms	UPS capacitor or battery momentarily supplies load; grid current catches up
Cooling Equipment Cycling	10–100 kW	0.1–5 s	Compressor or fan motor startup
Data Center Power Demand Ramp	0.5–5 MW	0.1–1 s	Load ramp due to synchronized IT workload or failover
Full Facility Change	Up to 10 MW step	10–100 ms	Sudden retransfer of load or UPS bypass event

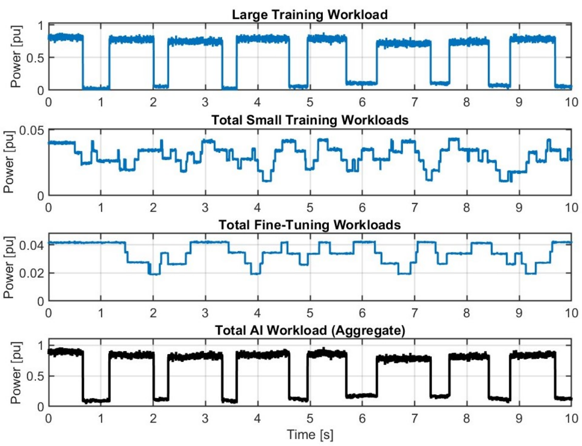

Fig. 1. AI Workload Profiles (scaled to 50 MW Nominal).

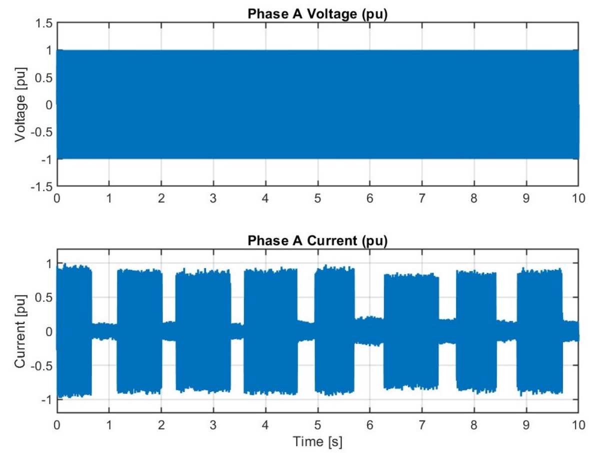

Fig. 2. Voltage and current waveforms during Data Center load changes.

Similarly, fine-tuning workloads operate at lower frequency f_1 with shorter tail and idle phases defined by analogous stochastic parameters:

$$T_{\text{ft},i} = \frac{1}{f_1(1+\zeta_i)}, \tag{8}$$

$$T_{\text{tail},i} = r_{\text{ft},i} T_{\text{ft},i}, \qquad T_{\text{idle},i} = (1 - r_{\text{ft},i}) T_{\text{ft},i}, \tag{9}$$

and

$$P_{\text{tail},i}(t) = P_{\text{ft}}\big(1 + \delta_{\text{tail},i} + \eta_{\text{tail}}(t)\big), \tag{10}$$

$$P_{\text{idle},i}(t) = P_{\text{ft}}\big(1 - \delta_{\text{idle},i} + \eta_{\text{idle}}(t)\big). \tag{11}$$

Fig. 1 illustrates the generated AI workload profiles scaled to the nominal 50 MW rating. The top three subplots depict the individual power variations for Large Training, Small Training, and Fine-Tuning workloads, exhibiting distinct stochastic patterns. The bottom subplot shows the aggregate power, highlighting the superposition of these cycles and the total variability seen by the grid. Corresponding to these power profiles, Fig. 2 displays the instantaneous Phase A voltage and current waveforms in per unit (pu). While the voltage remains relatively constant near 1.0 pu, the current exhibits rapid fluctuations and step changes that directly mirror the stochastic nature of the AI workloads shown in Fig. 1.

B. Aggregate Load Representation

The total power demand of the data center is expressed as the summation of all workloads:

$$P_{\text{AI,raw}}(t) = P_{\text{large}}(t) + \sum_{i=1}^{N_s} P_{\text{small},i}(t) + \sum_{j=1}^{N_f} P_{\text{ft},j}(t), \tag{12}$$

which is scaled to match a desired nominal power level $P_{\text{n,total}}$:

$$P_{\text{AI}}(t) = \alpha P_{\text{AI,raw}}(t), \qquad \alpha = \frac{P_{\text{n,total}}}{\max_t P_{\text{AI,raw}}(t)}. \tag{13}$$

The resulting profile captures both the short-term stochastic fluctuations and the longer-term periodicity of large-scale AI training cycles. When coupled with a network model, this dynamic power variation produces a time-varying apparent impedance:

$$Z_{\text{app}}(t) = \frac{V(t)}{I(t)} e^{j\phi(t)}, \tag{14}$$

where $\phi(t)$ is the instantaneous phase difference between voltage and current. This continuously changing impedance trajectory forms the basis for studying protection zone blurring and false tripping events in impedance-based relays. The specific stochastic parameters are listed in Table IV.

C. Model Parameters

This modeling framework allows the impedance-based protection study to incorporate realistic temporal power variations induced by AI workloads. The combination of Gaussian and uniform stochastic processes ensures that the synthetic profiles emulate realistic power consumption signatures of GPU clusters under training and inference operations, providing an accurate representation for dynamic impedance trajectory and relay maloperation analysis.

979-8-3315-8138-1

TABLE IV
PARAMETERS USED IN THE STOCHASTIC AI WORKLOAD MODEL

Symbol	Description	Value / Range	Unit
f_0	Baseline frequency (training)	0.5–1.5	Hz
f_1	Baseline frequency (fine-tuning)	0.3–0.7	Hz
σ_ξ	Duration variability (training)	0.1	–
$r_{tr,i}$	Compute phase ratio	0.55–0.8	–
μ_δ	Mean power difference between phases	0.9	–
σ_δ	Power variability	0.05	–
$\sigma_{\eta,up}$	Intra-phase variability (up)	0.035	–
$\sigma_{\eta,down}$	Intra-phase variability (down)	0.02	–
$r_{ft,i}$	Fine-tuning phase ratio	0.7–0.9	–
$\sigma_{\eta,tail}$	Intra-phase variability (tail)	0.02	–
$\sigma_{\eta,idle}$	Intra-phase variability (idle)	0.0125	–
P_{large}	Large training workload nominal power	9.0	p.u.
P_{small}	Small training workload nominal power	0.1	p.u.
P_{ft}	Fine-tuning workload nominal power	0.1	p.u.
$P_{\text{n,total}}$	Total data center rating	50	MW

IV. DYNAMIC IMPEDANCE TRACKING

Accurate impedance tracking during power swings is crucial for maintaining the stability and security of distance protection. During a dynamic load change, the apparent impedance $Z(t)$ can traverse the impedance plane rapidly, crossing multiple mho zones. This transient behavior challenges traditional steady-state blocking criteria, motivating the need for dynamic speed-based analysis of the impedance trajectory.

A. Simulation Test System

To evaluate the protection performance under dynamic load conditions, a radial line model was simulated. The system supplies a 50 MW data center load with a lagging power factor of 0.95. The line impedance is modeled as $Z_{\text{line}} = 1.0 + j1.6\ \Omega$, corresponding to a line angle of approximately $58°$. This realistic R/X ratio ensures the impedance trajectory behavior reflects typical transmission line characteristics rather than purely resistive load encroachment.

B. Impedance Estimation and Speed Analysis

To evaluate this behavior, the instantaneous apparent impedance was estimated from the measured phase voltage and current signals over moving windows corresponding to one fundamental cycle. To ensure physical validity for passive loads, the impedance calculation utilized the power-based method $R = P/I^2$ rather than pure phase angle extraction, preventing artifacts such as negative resistance during noisy low-current intervals. The apparent impedance is then given by

$$Z(t_k) = \frac{V}{I} e^{j\phi}. \tag{15}$$

To capture the dynamics of impedance movement during the power swing, the instantaneous rate of impedance change (or impedance speed) can compute as

$$\left| \frac{\Delta Z}{\Delta t} \right| = \frac{|Z(t_{k+1}) - Z(t_k)|}{\Delta t}, \tag{16}$$

which quantifies how rapidly the trajectory moves across the R–X plane. This metric provides an indicator for distinguishing slow load encroachment from fast-moving swings or transient faults. Fig. 2 illustrates the impedance speed via a heatmap color code on the trajectory. Fig. 3 provides a complementary time-domain view, plotting the perpendicular distance of the impedance from the line center. This plot explicitly visualizes the crossings of the outer and inner blinders, highlighting the duration of the impedance's presence within the protection corridor. The detection logic incorporates a 0.05s timing setting.

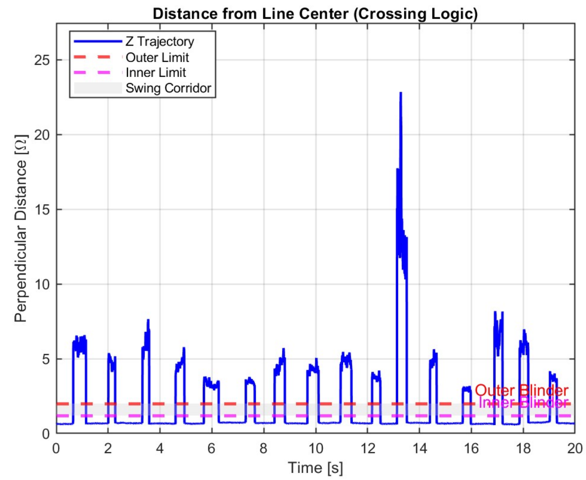

Fig. 3. Impedance Distance from Line Center and Blinder Crossing Logic.

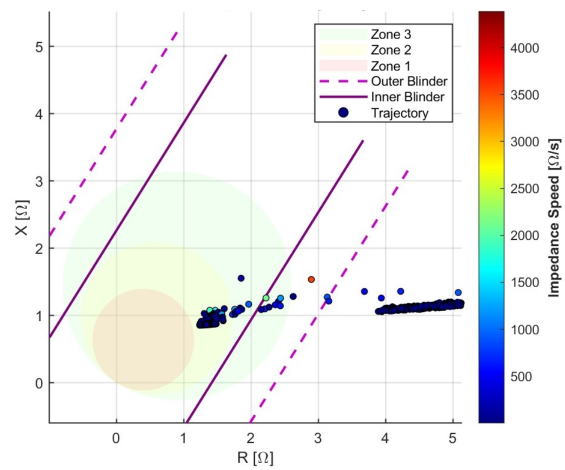

Fig. 4. Impedance Trajectory with Mho characteristics and PSB Blinders.

Fig. 4 presents the full impedance trajectory of the Data Center load in the R-X plane. The path shows the impedance entering the trip zone and then exhibiting the characteristic slow motion that leads to maloperation.

C. Maloperation Mechanism and Blinder Analysis

Traditional Power Swing Blocking (PSB) schemes often utilize blinders to detect slow-moving impedance trajectories. In this analysis, inner and outer blinders are placed as shown in Fig. 4.

Fig. 5 provides a unified analysis correlating the AI workload power (top), the apparent impedance magnitude (middle), and the protection logic (bottom). The bottom subplot details the crossing duration (Δt) for each event. Blue bars indicate "Slow Oscillations" where the crossing time exceeds the threshold, mimicking a power swing. Orange bars indicate

979-8-3315-8138-1

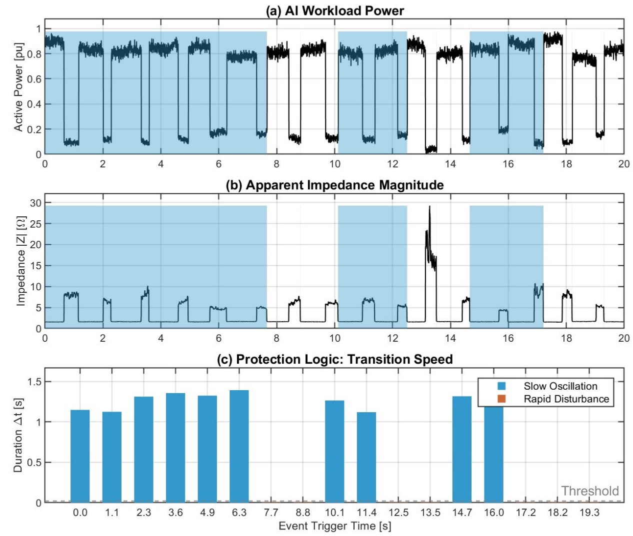

Fig. 5. Unified Analysis: Correlation of AI workload dynamics vs. protection response.

TABLE V
MHO ZONE AND SIMULATION PARAMETERS

Parameter	Symbol/Value	Description
System Voltage	$V_{LL} = 13.1$ kV	Nominal Line-to-Line Voltage
Fundamental frequency	$f_{\text{fund}} = 60$ Hz	System base frequency
Line Impedance	$Z_{\text{line}} = 1 + j1.6\ \Omega$	Line Angle $\approx 58^\circ$
Sampling period	Δt = 1 ms	Inverse of sampling frequency
Zone 1 radius	$r_1 = 0.8\lvert Z_{\text{line}}\rvert$	80% line reach (Instantaneous)
Zone 2 radius	$r_2 = 1.2\lvert Z_{\text{line}}\rvert$	120% line reach
Zone 3 radius	$r_3 = 1.8\lvert Z_{\text{line}}\rvert$	180% line reach
Outer Blinder Offset	1.4 Ω	Perpendicular to line angle
Inner Blinder Offset	1.0 Ω	Perpendicular to line angle
Simulation time	$T_{\max} = 60$ s	Shortened simulation horizon

"Rapid Disturbances" that resemble faults. As seen in the figure, the slow-moving oscillations (Blue) inside the zone persist for durations that can exceed typical protection time delays, leading to a trip. This confirms that traditional dynamic impedance tracking is unable to block these events due to the combination of fast entry and slow motion inside the trip characteristic.

Table V summarizes the key parameters used in the Mho-type distance protection simulation, including the system voltage, line impedance, and the blinder offsets.

This approach enables visualizing the impedance trajectory in the complex plane and quantifying its motion rate during system oscillations. While load encroachment conditions typically exhibit low $\left|\frac{\Delta Z}{\Delta t}\right|$, dynamic load changes can cause sharp excursions across multiple protection zones, as reflected by high impedance velocities. Hence, tracking $\left|\frac{\Delta Z}{\Delta t}\right|$ provides a useful metric for designing adaptive protection algorithms capable of stabilizing relay response during dynamic operating conditions. However, as seen in Figs. 4 and 5, the specific "Fast Entry, Slow Motion" behavior of Data Center loads defeats standard speed-based blocking, necessitating new discrimination methods.

V. CONCLUSION

This paper demonstrated that large and rapid load variations from modern Data Centers can drive the apparent impedance into the distance relay trip zone in a manner that mimics a true system fault. The dynamic impedance tracking results showed that the impedance trajectory enters the mho characteristic at very high speed but then slows dramatically once inside, a behavior that leads to power swing maloperation. Furthermore, the impedance speed analysis confirmed that these Data Center–induced dynamic load changes are not effectively blocked by traditional dynamic criteria, as their initial gradients exceed blocking thresholds while their steady behavior inside the trip zone resembles a stable swing. The addition of PSB blinders revealed that while some events are slow, the fast entry phase allows the impedance to bypass the detection logic, leading to zone entry. These findings indicate that existing distance protection schemes are vulnerable under such operating conditions. Consequently, new adaptive protection logic and discrimination methods are needed to reliably separate Data Center load surges from actual faults.

REFERENCES

[1] A. Jimenez-Ruiz and F. Milano, "Data center model for transient stability analysis of power systems," *arXiv*, vol. abs/2505.16575, 2025, preprint. [Online]. Available: https://arxiv.org/abs/2505.16575

[2] NERC Large Loads Task Force, "Characteristics and risks of emerging large loads: Large loads task force white paper," North American Electric Reliability Corporation (NERC), Tech. Rep., Jul. 2025, white Paper, Large Loads Task Force.

[3] D. Lumbreras *et al.*, "Trends in power quality, harmonic mitigation and active power filters," *Energies*, vol. 13, no. 21, p. 5792, 2020.

[4] G. E. Colon-Reyes, C. Tomlin, R. Dye, and D. Callaway, "Effects of dynamic power electronic load models on power systems analysis using zip-e loads," *arXiv*, vol. abs/2407.12715, 2024. [Online]. Available: https://arxiv.org/abs/2407.12715

[5] R. Jain, "Modern trends in power system protection for distribution," *Electric Power Systems Research*, vol. 215, p. 108832, 2022.

[6] P. Parikh, M. Ali, N. Virani, and S. C. Evans, "Strain to synergy: Powering ai data centers with sustainable and smart power grid infrastructures," in *Conference*, Sep. 2025, preprint / 2025 IEEE International Conference on Communications, Control, and Computing Technologies for Smart Grids (SmartGridComm).

[7] A. Mahari, M. Sanaye-Pasand, and S. M. Hashemi, "Adaptive phasor estimation algorithm to enhance numerical distance protection," *IET Generation, Transmission & Distribution*, vol. 11, no. 5, pp. 1170–1178, 2017.

[8] R. Vakili and M. Khorsand, "A machine learning-based method for identifying critical distance relays for transient stability studies," *arXiv*, vol. abs/2204.04395, 2022. [Online]. Available: https://arXiv.org/abs/2204.04395

[9] S. Sanati, A. Mosayebi, and I. Kamwa, "Advanced rapid directional over-current protection for dc microgrids using k-means clustering," *IEEE Transactions on Power Delivery*, vol. 39, no. 2, pp. 1088–1099, 2024.

[10] S. Biswas, A. C. Varghese, K. Chatterjee, S. Nekkalapu, B. Ross, and J. Follum, "Evaluating the risk to bulk power system reliability from large load induced oscillations," *TechRxiv (preprint)*, Aug. 2025, preprint.

[11] M. Ikhide, "Transient-based protection technique for future dc grids," *The Journal of Engineering*, vol. 2018, no. 18, p. 217–222.

[12] A. Arif, "Load modeling — a review," *Energy and Power Engineering*, vol. 9, no. 10, p. 359–368, 2017.

979-8-3315-8138-1